Environ Monit Assess (2020) 192: 717
https://doi.org/10.1007/s10661-020-08680-w

Evaluation of soil erosion and sediment deposition rates by the ^{137}Cs fingerprinting technique at different hillslope positions on a catchment

Yanqing Li · Zhongcheng Jiang · Yang Yu · Zhijie Shan · Funing Lan · Xiangfei Yue · Peng Liu · Yeboah Gyasi-Agyei · Jesús Rodrigo-Comino

Received: 12 May 2020 / Accepted: 13 October 2020 / Published online: 21 October 2020
© Springer Nature Switzerland AG 2020

Abstract Assessment of the variation of soil erosion and sediment mobilization at different hillslope positions using the ^{137}Cs tracing technique has been carried out for the Dapotou closed watershed, a representative depression in the karst gabin basin in Southwest China. The results showed that the annual soil erosion rates in the shoulders, backslopes, and footslopes were 0.87, 0.35 and 0.49 cm year^{-1}, respectively, while the soil sediment deposition rate in the depression bottom was 2.68 cm year^{-1}. The average annual soil erosion modulus of the complete hillslope was 632 t km^{-2}year^{-1}, which confirmed the seriousness of erosion according to the gradation of the karst soil erosion standards. For the whole catchment, the sediment delivery ratio was estimated as 0.82. To identify which factor could play the most important role in influencing the estimates using ^{137}Cs, a linear correlation and principal component analysis were conducted. The results showed that ^{137}Cs concentrations at different soil depths of the different hillslope positions were significantly correlated with soil organic matter and total nitrogen ($P < 0.05$). As this watershed is a typical karst geomorphological type, these findings are expected to provide data support for larger watershed soil erosion management and ecological restoration in fragile karst ecosystems.

Keywords Soil erosion · ^{137}Cs · Geomorphology · Karst gabin basin · Principal component analysis

Y. Li · Z. Jiang · F. Lan · X. Yue · P. Liu
Institute of Karst Geology, Chinese Academy of Geological Sciences, Guilin 541004, China

Y. Li · Z. Jiang · F. Lan · X. Yue · P. Liu
Key Laboratory of Karst Ecosystem and Treatment of Rocky Desertification, Guilin 541004, China

Y. Yu (✉)
School of Soil and Water Conservation, Beijing Forestry University, Beijing 100083, China
e-mail: theodoreyy@gmail.com

Z. Shan
Department of Sediment Research, China Institute of Water Resources and Hydropower Research, Beijing 100038, China

Y. Gyasi-Agyei
School of Engineering and Built Environment, Griffith University, Nathan, Queensland 4111, Australia

J. Rodrigo-Comino
Department of Physical Geography, University of Trier, 54296 Trier, Germany

J. Rodrigo-Comino
Soil Erosion and Degradation Research Group, Department of Geography, Valencia University, Blasco Ibàñez, 28, 46010 Valencia, Spain

Introduction

Soil erosion has been identified as a global geo-environmental hazard (Nearing et al. 2005; Salesa et al. 2019; Prise et al. 2009; Panagos et al. 2014). Due to the nutrient-poor characteristics of carbonate-rock parent materials, the effects of soil erosion are greater in karst areas, which occupy approximately 12% of global continental terrains (Febles-González et al.

2012). Of the global karst area of 22 million km^2, 15.6% is located in China, which accounts for 36% of its mainland. Karst areas in China are mainly concentrated in eight southwest provinces, namely Yunnan, Guizhou, Guangdong, Chongqing, Hunan, Hubei, Sichuan, and Guangxi (Jiang et al. 2014).

In karst areas, gabin basins and mountains usually coexist because of specific geological processes such as subsidence and dissolution of fault blocks induced by Cenozoic tectonic uplift among others (Wang et al. 2017). These differences in geomorphological characteristics, in addition to severe anthropogenic disturbance (e.g., agriculture), often produce a series of environmental problems (e.g., floods, erosion). In the gabin basins of China, studies on soil erosion and sediment yield of small catchments (10–10,000 ha) are limited. However, studies of small watersheds are paramount for understanding the linkages between soil erosion on hillslopes and sediment transport in large watersheds (Assefa et al. 2020; Schuller et al. 2004).

During the last two or so decades, many scholars have attempted to use ^{137}Cs to evaluate long-term soil erosion or soil sediment mobilization in karst areas, particularly on karst peak-cluster depressions and karst plateaus (Mabit et al. 2010; Bai et al. 2010; Feng et al. 2016; Luo et al. 2018). ^{137}Cs is an artificial radionuclide with a half-life of 30.17 years, which was released into the atmosphere during the thermonuclear weapon testing between the 1950s and 1970s (IAEA 2014). Traces of ^{137}Cs entered the earth's soils through dry and wet deposition, with the maximum deposition rate occurring in 1963 (Zhang et al. 2008a). It is a cost- and time-efficient tool for the evaluation of soil redistribution due to erosion and can complement the information provided by conventional erosion measurements (Lizaga et al. 2019) such as experiments involving natural or simulated rainfall (e.g., Gyasi-Agyei 2006; Fang et al. 2017; García-Díaz et al. 2017; Rodrigo-Comino et al. 2018). ^{137}Cs can provide retrospective estimates of long-term soil erosion and deposition rates without disturbing the soil environment by measuring equipment installations (Porto and Walling 2012; Mokhtari Karchegani et al. 2011). It can also be used to obtain detailed analyses of sediment migration on hillslopes (Rodrigo-Comino et al. 2016; Evans et al. 2019; Zebari et al. 2019).

In the small watersheds of eastern Yunnan, which have been adversely impacted by soil erosion, there is an urgent need to assess the sediment delivery ratio to inform policymakers and stakeholders about the potential land degradation processes and to recommend possible control measures. Therefore, the primary objective was to quantify the hillslope soil erosion, sediment mobilization, and sediment delivery in the closed depression watershed of the gabin basin of China using ^{137}Cs. Our study intended to detect the variations of ^{137}Cs and soil properties under different positions on the karst hillslopes, which could be considered a representative geological structure in southwest China. In addition, we attempted to quantify the impact of soil depth and hillslope position on soil erosion rates and analyzed the relationship between soil property variations and erosion rates using multivariate statistical techniques. The results obtained from this research would inform erosion and sediment control strategies for the whole watershed of the Yunnan karst gabin basin.

Materials and methods

Study area

The Dapotou depression is located in the Yangjie Town, Kaiyuan County, Yunnan Province of China, and bounded by longitudes 103° 17′ 25.63″–103° 18′ 3.40″ E and latitudes 23° 36′ 48.04″–23° 37′ 28.10″ N (Fig. 1). Its elevation ranges from 1267 to 1413 m a.s.l. and drains an enclosed depression area of 1.97 km^2. The underlying bedrock of the depression is a Triassic carbonate rock, which consists of Gejiu Group (T_2g) and Falang Group (T_2f) limestone. Most of the soils in this watershed are of clay-limestone texture.

This region experiences a subtropical monsoonal climate with two main seasons: a rainy season from June to September and a dry season from October to May (Jiang 2012). A unimodal rainfall regime with a mean annual precipitation of 904 mm, of which 80% occurs during the raining season, characterizes the region. The average annual temperature is 18.3 °C and the closest climate station is located at 103° 19′ 12.76″ E, 23° 37′ 17.25″ N. The soils in the study area are derived from the parent limestone material which has a high viscosity. The content of clay (< 2 μm), silt (2–50 μm), and sand (50–2000 μm) are 30.5%, 50.6%, and 18.9%, respectively (Li et al. 2020). The soil surface layer is generally thin and scattered with layers of C and B horizons directly connected with the carbonate rock. The affinity and adhesion between the rock and soil are very poor, thus being very unstable.

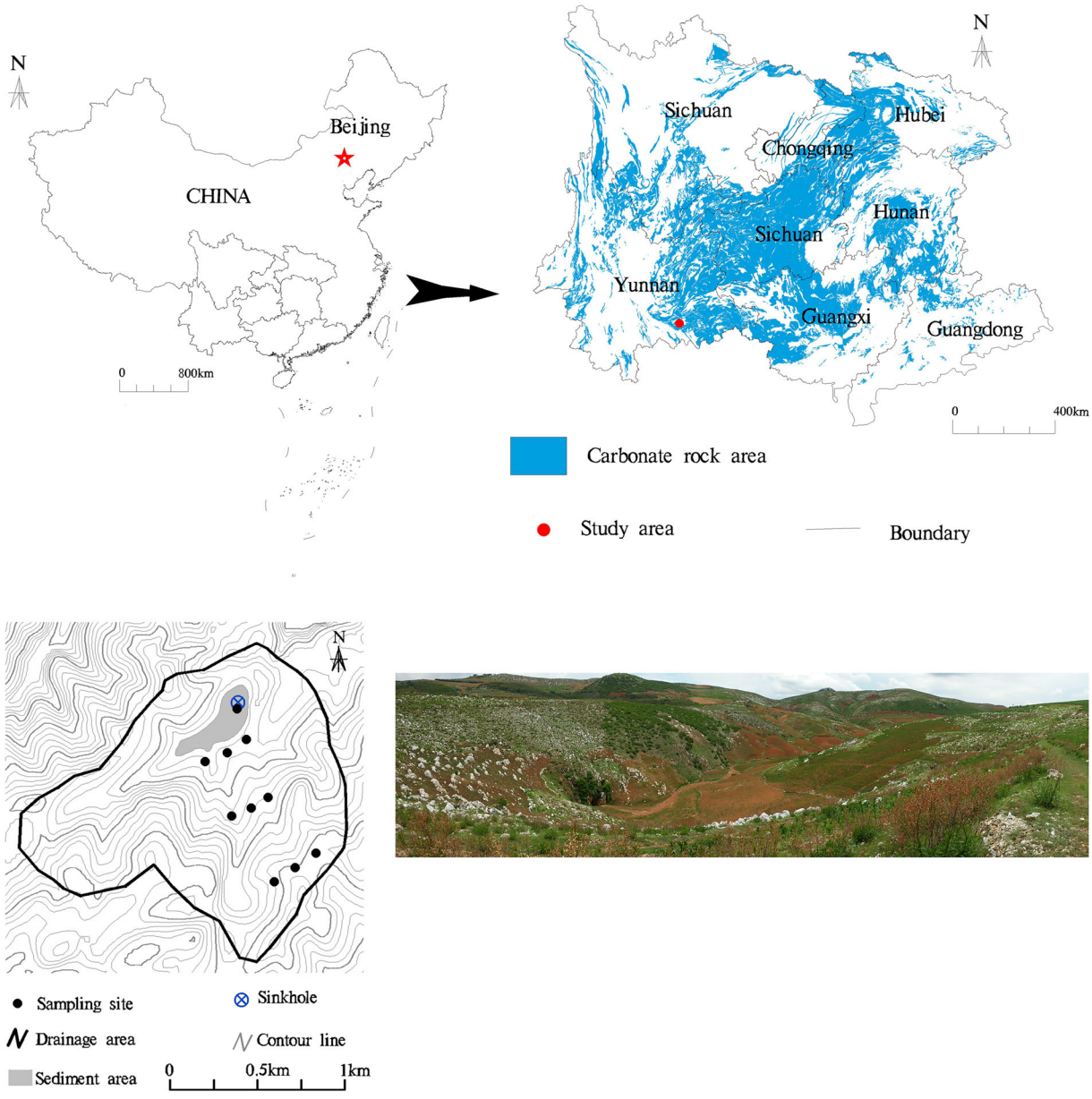

Fig. 1 Location of the study area (top panels), sampling points, and panoramic image of one selected plot (bottom panels)

The study area has a depression bottom with a length of about 1 km and an average width of about 60 m. Once-a-year, the hillslopes and depression bottom are cultivated with maize. There is a sinkhole in the northeast bottom of the depression (Fig. 1). Some hillslope areas are dominated by calcicole shrub and drought-tolerant herbs. When experiencing heavy rainfall, the bottom of the depression is submerged because the sinkhole is unable to discharge the total runoff immediately. Some of the generated runoff flows to the subterranean stream through the sinkhole. There are normally at least one or two flooding events during every rainy season.

Sampling tools and sampling design

In July 2017, soil samples were collected from 10 locations consisting of three each from three different cultivated hillslope (shoulder, backslope, and footslope) locations and one at the depression bottom (Fig. 1). At

each hillslope position, the soil samples were taken up to a depth of 40 cm, except for one backslope site at which the soil depth was limited to 30 cm deep, and at 240 cm depth for the depression bottom, to ensure that the full radionuclide soil content was taken into account. To establish the vertical distribution of ^{137}Cs, the samples were collected by using a scraper with 5 cm increments, giving a total of 70 soil samples from the hillslope locations and 48 soil samples from the depression. A cutting steel ring equipment was used to measure the bulk density of the soil samples in situ. The geographical coordinates and elevation of each sampling location were recorded using a GPS device. In the laboratory, the soil samples were sieved through a 2-mm sieve to remove plant roots and debris, then air-dried before performing the radionuclide and physicochemical property analysis.

A control plot was also established as a reference for the inventory site. Ideally, the land for the reference inventory should be flat and undisturbed. However, it was difficult to find any completely flat land which has not been cultivated since the mid-1950s. Therefore, local reference samples of ^{137}Cs were collected in a relatively flat shrub-grassland site (103° 26′ 48.37″ E, 23° 29′ 20.15″ N) 15 km from the study area. The reference site is well-vegetated, protected, and undisturbed as confirmed by the local elderly residents, and also from different periods remote sensing imagery. Five soil samples to a depth of 20 cm were collected from this reference site, and the average soil thickness of the reference profile was estimated as 20 cm.

Laboratory analysis

The ^{137}Cs analysis was performed at the Institute of Mountain Hazard and Environment, Chinese Academy of Sciences, laboratory. The ^{137}Cs content of the prepared samples weighing 300 g was measured by a Gamma-ray spectrometer using a hyper-pure coaxial germanium detector and multichannel analyzer system. ^{137}Cs was detected at 662 keV, and counting times were more than 50,000 s, providing results with an analytical precision of approximately ± 5% at the 95% level of confidence.

The soil physicochemical properties were measured at the Northwest Institute of Eco-Environment and Resources, Chinese Academy of Sciences. Soil organic matter (SOM) was determined by dry combustion at 500 °C (Davies 1974). Total nitrogen (TN) and total phosphorus (TP) concentrations were measured by using the persulfate digestion method. Total potassium (TK) was quantified by using the flame photometry method (Sparks et al. 1996). Finally, soil pH was analyzed by using a Mettler Toledo Seven Excellence pH meter.

Conversion models

The ^{137}Cs inventory of the soil profile at different hillslope positions was calculated using the following equation (Zhang et al. 2009a):

$$\mathrm{CPI} = \sum_{i=1}^{n} Ci \times \mathrm{Bd}i \times Di \times 10 \quad (1)$$

where CPI is the ^{137}Cs inventory (Bq m^{-2}) that represents the total amount of ^{137}Cs in the sample; i is the sampling layer sequence; n is the number of sampling layers; C_i is ^{137}Cs concentration (Bq kg^{-1}); Bd_i is the bulk density of a layer i (g cm^{-3}), and D_i is the depth of a layer i (cm).

The reference sample was considered using a bulk sample, i.e., without separation into 5-cm depth layers, and the ^{137}Cs inventory was calculated following Eq. (2) (Zhang et al. 2009a):

$$\mathrm{CPI} = Ci \times W \div S \quad (2)$$

where W is the weight of fine particles; S is the surface area of the sample plot.

It is widely used for the assessment of erosion rates which were estimated using the simplified Mass Balance Model equation for cultivated lands (Zhang et al. 1990) as:

$$A = A_0\left(1 - h \div H_p\right)^{N-1963} \quad (3)$$

where A_0 is the ^{137}Cs reference inventory (Bq m^{-2}); A is the ^{137}Cs inventory at an erosion point (Bq m^{-2}); h is the annual soil loss in depth since the year 1963 (cm); H_p represents the plow depth (cm); and N is the sampling year.

^{137}Cs has been widely used for dating of undisturbed soil profiles. The accepted ^{137}Cs depth profile is characterized by a single peak for the year 1963 when the ^{137}Cs maximum fallout flux occurred. The deposition rate since 1963 can be evaluated by using the following equation (Bai et al. 2010):

$$R = H_m/(n - 1963) \quad (4)$$

where R is the deposition rate (cm year^{1}), H_m is the depth of the peak in ^{137}Cs activity (cm), and n is the sampling year.

The deposited sediments used to be mixed into the top layer by plowing activities at the karst depression bottom. The ^{137}Cs distribution depth at the depression bottom is greater than the local reference inventory. Under the assumption that ^{137}Cs fallout was totally on the ground in 1963, the sediment deposition depth was derived from the equation (Bai et al. 2010):

$$\Delta H = H_t - H_p \quad (5)$$

where ΔH is the sediment deposition depth since 1963 (cm), H_t represents the total ^{137}Cs distribution in the profile (cm), and H_p is the plow layer depth (cm).

The modulus of soil erosion is calculated as (Zhang et al. 2008b):

$$Y = h \times D \times 10,000 \quad (6)$$

where Y is the soil erosion modulus (t km^{-2}year^{-1}); D is the soil density (g cm^{-3}).

We calculate soil delivery ratio (r) as:

$$r = 1 - Q_d / Q_m \quad (7)$$

where Q_d is the total deposition amount (t) and Q_m is the total erosion amount (t).

Statistical analysis

Data on soil pH, SOM, TN, TP, and TK were statistically analyzed to provide annual averages for each soil depth under the different hillslope positions (shoulder, backslope, and footslope). Analysis of variance (ANOVA) was conducted on soil properties and sediment deposition rates to evaluate their statistical differences at different hillslope positions and depths. To obtain significant differences at $P < 0.05$, the variable means were compared using an LSD (least significant difference) test. A Pearson correlation and principal component analysis (PCA) were also performed to first determine the correlations among the measured variables, and to help reduce the number of studied factors involved in the interaction between soil erosion and properties. The raw datasets were standardized before the analysis, and all statistical analyses were conducted using the R software (version 4.00) and vegan package.

Results

Variation of ^{137}Cs and soil physicochemical properties at different hillslope positions

Comparing the means, the results showed that ^{137}Cs concentrations were significantly different at the different hillslope positions ($P < 0.05$) (Fig. 2). On average, the backslopes showed the highest ^{137}Cs concentrations (0.83 ± 0.54 Bq kg^{-1}), followed by the footslopes (0.58 ± 0.23 Bq kg^{-1}) and then the shoulders (0.20 ± 0.09 Bq kg^{-1}). The ^{137}Cs inventories at the backslope, footslope, and shoulder hillslope positions were, respectively, 364.6 Bq m^{-2}, 249.9 Bq m^{-2}, and 85.1 Bq m^{-2}, the overall mean being 226.5 Bq m^{-2}.

Similar to the ^{137}Cs concentrations, we found that the maximum values of soil pH, SOM TN, TP, and TK occurred in the backslope hillslope positions. Also, it is important to remark that soil pH, TN, and TK were higher in the shoulders than in the footslopes, while SOM and TP were higher in the backslopes and footslopes than in the shoulders. Except for SOM, other soil properties (pH, TN, TP, and TK) were significantly different at the different hillslope positions (Table 1).

Variation of ^{137}Cs and soil physicochemical properties at different soil depths

Figure 2 and Table 2 show the variations of ^{137}Cs concentrations and soil properties for the selected hillslopes and different soil depths, respectively. In the shoulder positions, ^{137}Cs was mainly distributed in the topsoil (i.e., 0.38 Bq kg^{-1} in 0–5 cm and 0.89 Bq kg^{-1} in 5–10 cm soil). For depths below 10 cm, ^{137}Cs concentration decreased rapidly. There were no ^{137}Cs detected in the 15–20-cm and 25–40-cm soil depth layers.

For the backslope positions, ^{137}Cs concentration ranged from 0.23 to 1.32 Bq kg^{-1}, mainly distributed within the top 15-cm soil depth (i.e., 1.06 Bq kg^{-1} in 0–5 cm, 1.32 Bq kg^{-1} in 5–10 cm, and 1.30 Bq kg^{-1} in 10–15-cm soil). The mean ^{137}Cs concentration of the whole soil profile was 0.83 Bq kg^{-1}.

As for the footslope positions, the ^{137}Cs concentration was mainly distributed within the top 10-cm soil depth. The peak concentration of ^{137}Cs occurred in the 0–5 cm with 1.61 Bq kg^{-1}. From the top 5 cm, ^{137}Cs concentration decreased with increasing soil depth. There were no detections of ^{137}Cs in the 25–30-cm

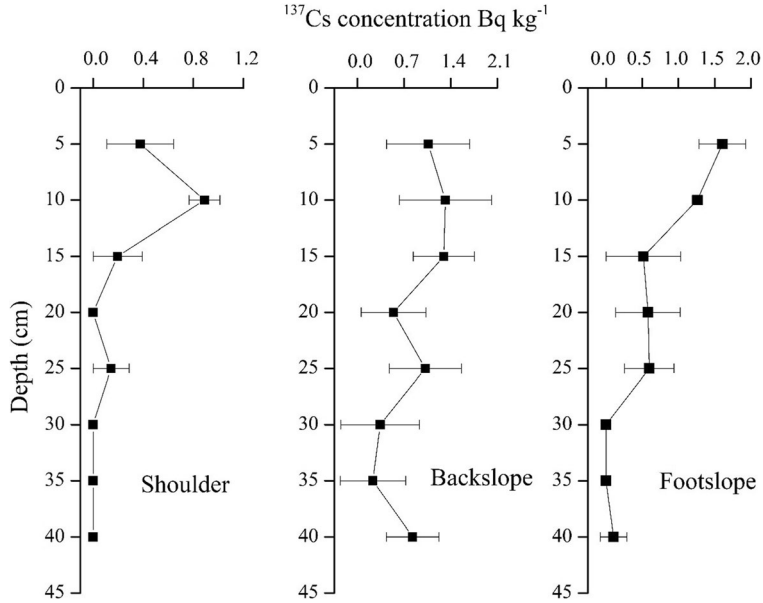

Fig. 2 ^{137}Cs concentration distribution at different hillslope positions and soil depths

and 30–35-cm soil depths, the mean concentration in the footslope positions being 0.58 Bq kg^{-1}.

Based on the variance analysis of the five soil depths (0–5 cm, 5–10 cm, 10–20 cm, 20–30 cm, and 30–40 cm), ^{137}Cs concentration was significantly different ($P < 0.05$). Multiple comparisons showed ^{137}Cs concentration in 0–5-cm layer was significantly higher than those below 10 cm depth. ^{137}Cs concentration in the 5–10-cm layer was significantly different from those in the 10–20-cm, 20–30-cm, and 30–40-cm depth layers, but it was not significantly different from the 0–5-cm depth layer concentration. ^{137}Cs concentrations in the 10–20-cm, 20–30-cm, and 30–40-cm depth layers showed no significant differences.

Some soil properties (SOM, TN, TP) showed significant differences ($P < 0.05$) at the different soil depths, while TK and pH showed no significant differences among the soil depth layers. SOM showed significant decreases with depth, namely 0–5-cm (1.89 g kg^{-1}), 5–10-cm (1.40 g kg^{-1}), 20–30-cm (0.88 g kg^{-1}), and 30–40-cm (0.62 g kg^{-1}) layers. TN in 0–5 cm (0.16 g kg^{-1}) was significantly higher ($P < 0.05$) than the soil layers below 10 cm but had no significant difference with the 5–10-cm soil depth layer. TP in 0–5 cm (0.033 g kg^{-1}) and 5–10 cm (0.035 g kg^{-1}) was significantly higher ($P < 0.05$) than that in the soil depth layers below 20-cm. Soil TP had no significant differences between two adjacent soil depths.

^{137}Cs variation of depression bottom at different soil depths

We observed a general trend in ^{137}Cs concentration in the depression bottom (Fig. 3), namely an initial increase with soil depth, and then a progressive decrease. The peak of ^{137}Cs concentration was observed in the 165-cm soil layer (2.38 Bq kg^{-1}), while the mean in the

Table 1 Average of ^{137}Cs concentrations and soil properties at different hillslope positions

	^{137}Cs Bq kg^{-1}	pH	SOM g kg^{-1}	TN g kg^{-1}	TP g kg^{-1}	TK g kg^{-1}	Slope gradient (°)
Shoulder	0.20 ± 0.09b	6.87 ± 0.37b	0.95 ± 0.72a	0.09 ± 0.04b	0.02 ± 0.00b	1.06 ± 0.21b	27
Backslope	0.82 ± 0.54a	7.47 ± 0.74a	1.27 ± 0.52a	0.14 ± 0.05a	0.03 ± 0.01a	1.95 ± 0.54a	20
Footslope	0.58 ± 0.23a	6.09 ± 1.03c	1.05 ± 0.32a	0.09 ± 0.03b	0.03 ± 0.01b	0.95 ± 0.34b	23

Data represent means and standard deviations (SD). Different lowercase letters indicate a significant difference among slope positions; the same letter means no significant differences

Table 2 Average variations in ^{137}Cs concentrations and soil properties at different soil depths

	^{137}Cs Bq kg^{-1}	pH	SOM g kg^{-1}	TN g kg^{-1}	TP g kg^{-1}	TK g kg^{-1}
0–5 cm	1.01 ± 0.67a	6.31 ± 1.02a	1.89 ± 0.87a	0.16 ± 0.05a	0.033 ± 0.007a	1.37 ± 0.63a
5–10 cm	1.16 ± 0.41a	6.49 ± 1.06a	1.40 ± 0.32b	0.13 ± 0.03ab	0.035 ± 0.011a	1.33 ± 0.68a
10–20 cm	0.52 ± 0.54b	6.82 ± 0.95a	1.04 ± 0.27bc	0.10 ± 0.04bc	0.028 ± 0.009ab	1.33 ± 0.62a
20–30 cm	0.35 ± 0.39b	7.06 ± 0.87a	0.88 ± 0.33c	0.09 ± 0.04 cd	0.022 ± 0.006bc	1.26 ± 0.60a
30–40 cm	0.09 ± 0.14b	5.73 ± 2.58a	0.62 ± 0.34c	0.06 ± 0.04d	0.018 ± 0.009c	1.07 ± 0.61a

Data represent means and standard deviations (SD). Different lowercase letters indicate a significant difference among different depths ($P < 0.05$); the same letter means no significant differences

whole depression soil profile was 1.25 Bq kg^{-1}, higher than the values of the tested hillslope positions.

The potential connection between soil properties and sediment deposition rates

The Pearson correlation and principal component (PC) analysis (PCA) were carried out on the variables related to sediment deposition rates using ^{137}Cs (Table 3). The highest linear correlation ($P < 0.05$) was found for SOM (0.669), N (0.643), and P (0.620). Figure 4 shows a plot of the eigenvector in the plane of the first two PCs together with their PC scores, PC1 explaining 61.4% of the total variance and PC2 23.6%. ^{137}Cs is significantly influenced by hillslope positions and closely related to SOM and TN. The linear correlation between ^{137}Cs and SOM is depicted in Fig. 5.

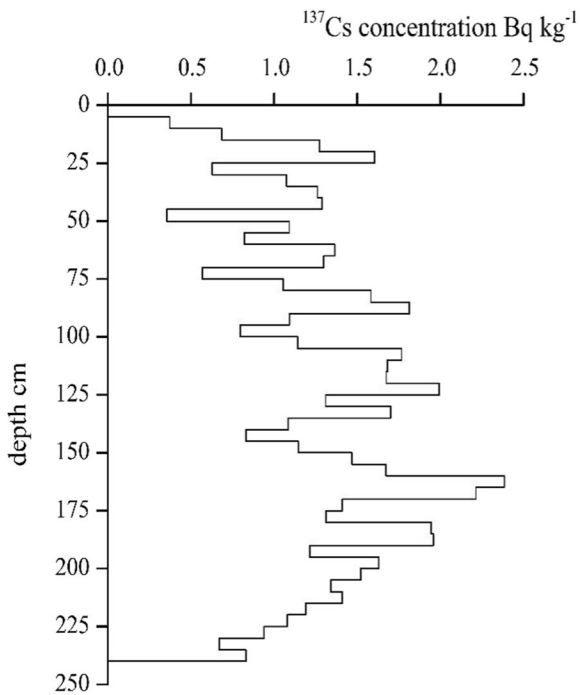

Fig. 3 ^{137}Cs concentration distribution with depth in the depression bottom

Soil erosion modulus estimation

For the reference (control) site, soil samples of all depths were lumped together, i.e., without separating the layers. The average ^{137}Cs concentration at the reference site was 6.28 Bq kg^{-1}. The surface area of each sample plot was 0.01 m^2 and the average weight for the fine particles smaller than 2 mm was 1.5 kg. Using Eq. (2), we obtained 942 Bq m^{-2} as the reference value for ^{137}Cs inventory. The ^{137}Cs inventories at the different hillslope positions (shoulder, backslope, footslope) were lower than the reference plot inventory, indicating the possibility of soil erosion happening in the disturbed hillslopes. Calculating the soil erosion rates using Eq. (3), the annual average soil erosion rates in the

Table 3 Principal component analysis of the potential connection between soil properties and sediment deposition rates

Principal component	PC-1	PC-2
Eigenvalues	0.18	0.07
Variance (%)	61.42	23.64
Cumulative (%)	61.42	85.06
CS	0.52	− 0.65
pH	0.24	0.48
SOM	0.31	− 0.12
TN	0.45	− 0.03
TP	0.44	0.07
TK	0.42	0.57

PC-1 and PC-2 indicate first principal component and second principal component, respectively

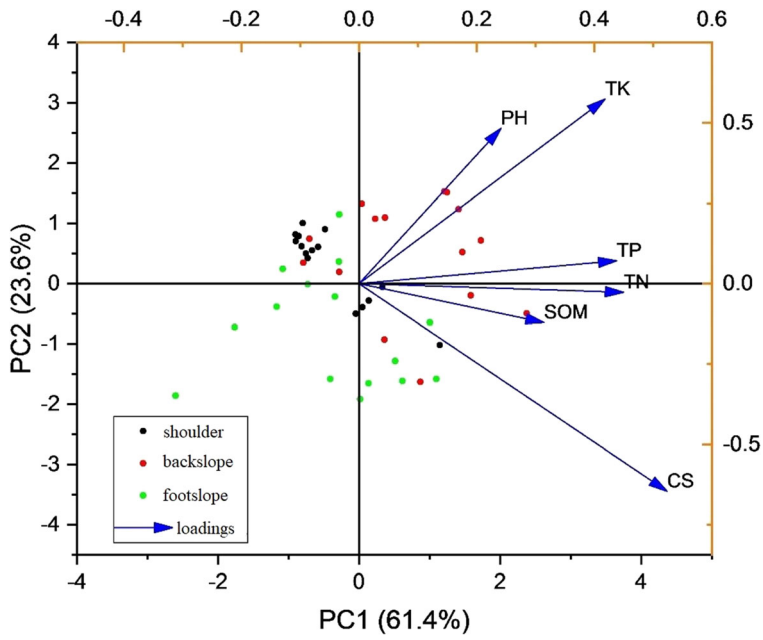

Fig. 4 Eigenvectors from the principal component analysis (PCA) of the first two components (PC1 and PC2)

shoulders, backslopes, and footslopes were 0.87 cm year^{-1}, 0.35 cm year^{-1}, and 0.49 cm year^{-1}, respectively. The soil erosion modulus from Eq. (6) gave an average erosion modulus value for the whole hillslope as 632 t km^{-2}year^{-1}.

In the depression bottom, the ^{137}Cs distribution was much deeper than that of the reference depth and the plow layer, and the ^{137}Cs inventory was much greater than the ^{137}Cs reference inventory. Based on the depression bottom ^{137}Cs peak concentration value at the 165-cm soil depth layer, the deposition depth since 1963 was estimated as 145 cm because the local plow layer depth is about 20 cm. From Eq. (4) and Eq. (5), we obtained the average deposition rates since 1963 as 2.68 cm year^{-1}.

Discussion

Choosing a reference plot was a critical step for assessing the soil erosion rates using the ^{137}Cs

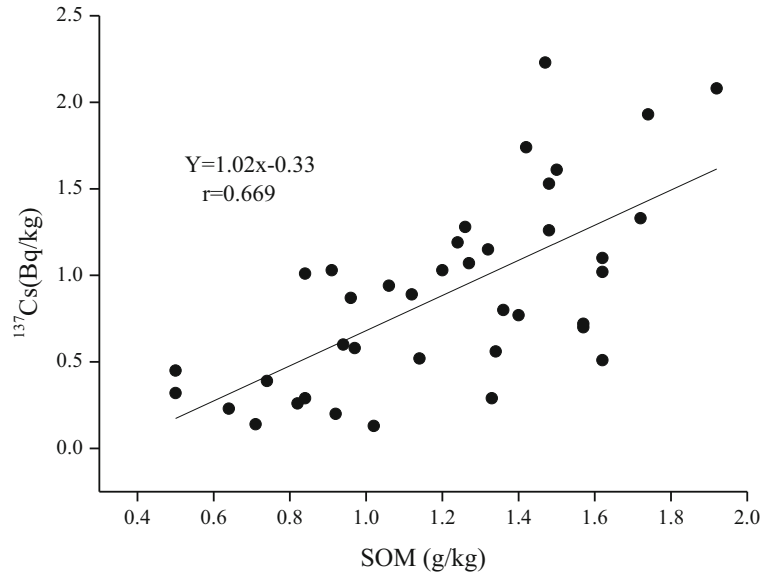

Fig. 5 Linear correlation between ^{137}Cs and SOM (soil organic matter) content

fingerprinting technique. Some researchers have doubted this methodology because of ^{137}Cs fallout heterogeneity (Parsons and Foster 2011; Bazshoushtari et al. 2016). It is well-known that ^{137}Cs fallout can be influenced by rainfall and latitude. Although the reference site is located only 15 km away, its rainfall and latitude are consistent with the plot sites. The reference inventory in the study site was 942 Bq m^{-2} which is close to the values of previous studies under similar rainfall and latitude conditions. For example, Zhang et al. (2009b) used 918 Bq m^{-2} as the ideal reference inventory plot value in the Dianchi watershed while Xiong et al. (2018) used 906 Bq m^{-2} as the reference inventory in the Shilin county; both study sites are located in the Yunnan province. The year of 1954 is rather known as the onset of ^{137}Cs fallout than a high fallout deposition year. We can highlight the large uncertainty on the reference 1963 fallout peak position which is somewhere between the 150- and 200-cm soil depth. It could be due to soil particle mixing as a result of land cultivation or to a more complex deposition trend including a varying supply of ^{137}Cs-attached soil particles. Therefore, any deposition rate derived from this soil depth may be questionable. More soil sampling, or in situ measurements, needs to be performed to reduce this uncertainty (Li et al. 2011).

Normally, soil erosion is greatest in the shoulder, followed by the backslope and lowest in the footslope as other authors observed in other Asian countries and Mediterranean belt (Mokhtari Karchegani et al. 2011; Rahimi et al. 2013; Ayoubi et al. 2012). In this study, soil erosion is greater in the shoulder followed by the footslope and then the backslope. The steeper gradient of the shoulder compared to the backslope could explain this finding. Lu et al. (2016) showed that the slope gradient is a key factor affecting soil erosion where rainfall and vegetation coverage are not varying. However, other studies have suggested that steep bare soil subjected to high-intensity rainfall could be rapidly transformed from a loose seedbed to a crusted surface with pronounced micro-relief, as observed in a study in northern Laos (Ribolzi et al. 2011). In our research area, the geological and vegetation conditions are possibly playing roles in different ways; therefore, our findings do not corroborate other published research. Perhaps, the correlations observed in our study and the reduction of factors using the PCA may not be directly related to ^{137}Cs adsorption by soil organic matter, but rather to the fact that soil micro-aggregates contain both organic matter and ^{137}Cs bound to fine clay minerals. In the long term, erosion could deplete the topsoil horizons of both soil organic matter and ^{137}Cs bound particles during soil aggregate breakdown. On the backslope, chemical dissolution is strong, forming some relatively closed microtopography, such as lapies and solution pans. Soil from the shoulder is easily deposited into these micro topographical forms (Zhang et al. 2009b). Another possible reason is the coexistence between tillage and water erosion which could play key roles as the main cause of soil loss at the concave position (Lobb and Kachanoski 1999), i.e., the shoulder position (upper parts), while water erosion could lead to serious soil loss at footslope positions due to maximum runoff concentrations. However, other research carried out in steep and conventionally tilled managed fields have highlighted the importance of soil management practices conducted by handmade tillage or tractor passes redistributing soil sediments along the hillslopes (Afshar et al. 2010; Cerdà and Rodrigo-Comino 2020). This issue is closely related to the connectivity processes; thus, using this method could provide an estimate only (López-Vicente et al. 2015; Parsons et al. 2015; Smetanová et al. 2018). Using other techniques and increasing the number of samples, this factor could be properly studied and its influence deciphered.

Following the trend in soil erosion observed in our results, ^{137}Cs concentrations peaked in the 5–10-cm soil depth layer in the shoulders and footslopes, but only in the first 5-cm soil depth layer of the backslopes. These results implied that soil erosion is highly affecting the topsoil layers, which is a serious issue, specifically, in the shoulders and footslopes. On the contrary, the microtopography that is formed in the backslopes could capture the soil particles carried by erosion from the shoulders, which could be responsible for the elevated ^{137}Cs concentration in the soil surface.

Our findings also showed that the ^{137}Cs concentrations of different soil depth layers were significantly correlated with SOM. These results are consistent with previous studies conducted under different environmental conditions (Parsons and Foster 2011). This connection has a significant impact on the pathways of ^{137}Cs movement in the near-surface environment (Agapkina et al. 1995). In soil profiles, the concentration of ^{137}Cs shows a discontinuous trace distribution with depths. On one hand, there could be the possibility of soil creeping in the soil and rock interfaces affecting the parent material (i.e., the carbonate rocks in this study)

composition. On the other hand, ^{137}Cs is mainly adsorbed by the fine soil particles and soil organic matter. The fine soil particles are easily mobilized to deeper soil layers under the action of gravity and leaching of rainwater.

The soil erosion modulus average value of 632 t $km^{-2}year^{-1}$ was much higher than the karst peak-cluster area in the Longhe village, Guangxi Province area studied by Luo et al. (2018). On the one hand, some soil erosion control treatments and prevention measures were said to have made great progress in reducing the soil erosion modulus by about 500 t $km^{-2}year^{-1}$ from 2003 to 2015 (Luo et al. 2018). However, the soil in peak-cluster depressions was thinner and some areas had no soils, just bedrocks owing to antecedent soil erosion epochs. To understand the extent of soil erosion in our study site, we used the standard procedures established by Cao et al. (2008) who calculated the carbonate rock soil formation rate by analyzing the factors influencing soil formation. Related to the sampling location, the study was conducted at a small closed catchment (1.97 km^2). Therefore, we prefer to use a typical hillslope position sampling to conduct our assessment to decrease the heterogeneity. We believe it is better to get a general overview of this small catchment-scale as other authors have done (Bai et al. 2010; Zhang et al. 2010, etc.). Cao et al. (2008) used soil formation rates as soil loss tolerance and redefined the classification standard of the intensity of soil and water losses in the karst area into the following categories: very slight (< 30), slight (30–100), medium (100–200), serious (200–500), very serious (500–1000), and severe (> 1000 t km^{-2} $year^{-1}$). Based on the abovementioned classification, our research site was very seriously eroded, which would require corrective measures to mitigate soil erosion.

At the study site, considering the different soil erosion rates and the proportions of the area of the different hillslope positions, the annual total soil loss was about 1207 t. According to the sediment rates and depression bottom areas, the annual total soil sediment deposition reached only 213 t. In the same closed catchment, the soil eroded is much more than deposited. This indicated that part of the eroded soil from the hillslopes could be transported to the subterranean stream through the sinkhole in the northeast of the bottom of the depression. From the erosion and sediment rate difference, we worked out the sediment delivery ratio in our study site to be about 0.82. This result is greater than the empirical value of reasonable sediment delivery ratio (0.7) obtained by Zhang et al. (2010) using the DEPOSITS model. Ward et al. (1981) proposed the DEPOSITS model for estimating sediment delivery ratio in small impoundments based on the plug flow theory. The DEPOSITS model assumes that the sediment delivery ratio is in proportion to runoff retention time. In karst areas, depressions can be considered temporary impoundments because the area is easily flooded (Wang et al. 2004b). At the same time, the plug flow theory only considers flooded conditions. Nowadays, there are many rainfall events which do not lead to flooding at the study site. Therefore, calculating the sediment delivery ratio that considers local conditions could be more reliable than the generic empirical value.

The depression is a typical geomorphic unit of karst gabin basin. There are a great number of depressions in the karst gabin basin which are the major soil erosion areas. When soil erosion happens in the studied hillslope after a rainfall event, the soil loss is divided into two parts according to the sediment delivery ratio; 18% of soil loss is deposited in the depression bottom, and 82% is transported to the subterranean stream system. The sediments which flowed into the subterranean stream are also divided into two parts. One part of the transported sediments is deposited in the subterranean conduit and the rest is discharged from the subterranean stream system. The sediment delivery ratio in the subterranean system is a challenging and meaningful investigation warranting further research. Because soil erosion mainly happens on the cultivated hillslopes, biological measures such as afforestation using deep-rooted species should be prioritized. Also, to encourage the shift in crop selection, high-value perennial crops or using mulches should be promoted (Rodrigo-Comino et al. 2020). Deep and intensive tillage should be reduced or avoided to further reduce soil compaction and the destruction of aggregates (Marques et al. 2020). Finally, growing plant fences or building sediment storage dams in front of the sinkholes could also minimize soil loss. All of this, considering future potential scenarios where climate change could vary the current conditions studied in this investigation (Akter et al. 2018; Rayamajhi and Manandhar 2020; Wang et al. 2004a).

Conclusions

The distribution of ^{137}Cs in different hillslope positions (shoulder, backslope, and footslope) of a typical karst

depression (Dapotou closed watershed, Southwest China) has been used to estimate soil erosion, sediment mobilization, and the overall sediment delivery ratio of the depression. It was observed that ^{137}Cs concentrations were significantly different at the different hillslope positions, the highest concentration occurring at the backslope and lowest at the shoulder. Also, the top 5-cm soil layer of the shoulder hillslope position exhibited the highest concentration decreasing rapidly with soil depth, while for the backslope and footslope positions, the concentration was in the top 15-cm and 10-cm layer, respectively. With respect to the depression area, the concentration was observed in the top 165-cm soil layer, but the average concentration values were higher than the hillslope positions. A strong correlation was found between ^{137}Cs concentrations and some soil properties, particularly the soil organic matter. The annual average soil erosion rate was highest for the shoulder that exhibited the lowest ^{137}Cs concentration, followed by the footslope. The main driving factors of ^{137}Cs concentration distribution, and erosion rates, were the micro topographical changes, the strong slope gradients, and the intensive tillage practices. To reduce soil erosion in this region, we recommend implementation of erosion control measures that are feasible and can be easily implemented by the stakeholders.

Acknowledgments Valuable contributions by Dr. Ruirui Cheng and Dr. Fan Liu from the Institute of Karst Geology and many others are greatly appreciated. Finally, we appreciate the editor and two anonymous reviewers' constructive comments and suggestions.

Funding This work was jointly funded by the National Key Research and Development Program (Evolution, integrating treatment and technological demonstration of rocky desertification in Karst Gabin Basin, Grant No. 2016YFC0502503), the Guangxi Natural Science Foundation (Grant Nos. 2017GXNSFBA198037; 2017JJA150639y), the National Natural Science Foundation of China (Grant No. 41502342), and the Guangxi Key Research and Development Program (GuikeAB110004). Yang Yu received the Young Elite Scientist Sponsorship Program by the China Association for Science and Technology (2017–2019).

References

Afshar, F. A., Ayoubi, S., & Jalalian, A. (2010). Soil redistribution rate and its relationship with soil organic carbon and total nitrogen using ^{137}Cs technique in a cultivated complex hillslope in western Iran. *Journal of Environmental Radioactivity, 101*(8), 606–614. https://doi.org/10.1016/j.jenvrad.2010.03.008.

Agapkina, G. I., Tikhomirov, F. A., & Shcheglov, A. I. (1995). Association of Chernobyl-derived 239+240Pu, 241Am, 90Sr and ^{137}Cs with organic matter in the soil solution. *Journal of Environmental Radioactivity, 29*, 257–269.

Akter, T., Quevauviller, P., Eisenreich, S. J., & Vaes, G. (2018). Impacts of climate and land use changes on flood risk management for the Schijn River, Belgium. *Environmental Science & Policy, 89*, 163–175.

Assefa, F., Elias, E., Soromessa, T., & Ayele, G. T. (2020). Effect of changes in land-use management practices on soil physicochemical properties in Kabe Watershed, Ethiopia. *Air, Soil and Water Research, 13*, 1178622120939587. https://doi.org/10.1177/1178622120939587.

Ayoubi, S., Ahmadi, M., Abdi, M. R., & Abbaszadeh Afshar, F. (2012). Relationships of 137Cs inventory with magnetic measures of calcareous soils of hilly region in Iran. *Journal of Environmental Radioactivity, 112*, 45–51. https://doi.org/10.1016/j.jenvrad.2012.03.012.

Bai, X. Y., Zhang, X. B., Chen, H., & He, Y. B. (2010). Using Cs-137 fingerprinting technique to estimate sediment deposition and erosion rates from Yongkang depression in the karst region of Southwest China. *Land Degradation & Development, 21*, 474–479. https://doi.org/10.1002/ldr.983.

Bazshoushtari, N., Ayoubi, S., Abdi, M. R., & Mohammadi, M. (2016). Variability of (137)Cs inventory at a reference site in west-central Iran. *Journal of Environmental Radioactivity, 165*, 86–92. https://doi.org/10.1016/j.jenvrad.2016.09.010.

Cao, J. H., Jiang, Z. C., Yang, D. S., Pei, J. G., Yang, H., & Luo, W. Q. (2008). Soil loss tolerance and prevention and measurement of karst area in southwest China. *Soil and water conservation in China, 12*, 40–45.

Cerdà, A., & Rodrigo-Comino, J. (2020). Is the hillslope position relevant for runoff and soil loss activation under high rainfall conditions in vineyards? *Ecohydrology & Hydrobiology, 20*(1), 59–72. https://doi.org/10.1016/j.ecohyd.2019.05.006.

Davies, B. E. (1974). Loss-on-ignition as an estimate of soil organic matter. *Soil Science Society of America Journal, 38*(1), 150–151. https://doi.org/10.2136/sssaj1974.03615995003800010046x.

Evans, D. L., Quinton, J. N., Tye, A. M., Rodés, Á., Davies, J. A. C., Mudd, S. M., & Quine, T. A. (2019). Arable soil formation and erosion: a hillslope-based cosmogenic nuclide study in the United Kingdom. *SOIL, 5*(2), 253–263. https://doi.org/10.5194/soil-5-253-2019.

Fang, N. F., Wang, L., & Shi, Z. H. (2017). Runoff and soil erosion of field plots in a subtropical mountainous region of China. *Journal of Hydrology, 552*, 387–395. https://doi.org/10.1016/j.jhydrol.2017.06.048.

Febles-González, J. M., Vega-Carreño, M. B., Tolón-Becerra, A., & Lastra-Bravo, X. (2012). Assessment of soil erosion in karst regions of Havana, Cuba. *Land Degradation & Development, 23*(5), 465–474. https://doi.org/10.1002/ldr.1089.

Feng, T., Chen, H., Polyakov, V. O., Wang, K., Zhang, X., & Zhang, W. (2016). Soil erosion rates in two karst peak-cluster depression basins of northwest Guangxi, China: Comparison of the RUSLE model with 137Cs measurements. *Geomorphology, 253*, 217–224. https://doi.org/10.1016/j.geomorph.2015.10.013.

García-Díaz, A., Bienes, R., Sastre, B., Novara, A., Gristina, L., & Cerdà, A. (2017). Nitrogen losses in vineyards under

different types of soil groundcover. A field runoff simulator approach in central Spain. *Agriculture, Ecosystems & Environment, 236*, 256–267.

IAEA (International Atomic Energy Agency). (2014). *Guidelines for using fallout radionuclides to assess erosion and effectiveness of soil conservation strategies, IAEA-TECDOC-1741* (p. 213). Vienna: IAEA publication.

Jiang, Y. (2012). Sources of sulfur in the Nandong underground river system, southwest China: a chemical and isotopic reconnaissance. *Applied Geochemistry, 27*, 1463–1470. https://doi.org/10.1016/j.apgeochem.2012.05.001.

Jiang, Z., Lian, Y., & Qin, X. (2014). Rocky desertification in Southwest China: impacts, causes, and restoration. *Earth-Science Reviews, 132*, 1–12. https://doi.org/10.1016/j.earscirev.2014.01.005.

Li, H., Zhang, X., Wang, K., & Wen, A. (2011). ^{137}Cs redistribution in thin stony soil of a carbonate rock slope in Southwest China. *Pedosphere, 21*(1), 37–45.

Li, Y. Q., Jiang, Z. C., Chen, Z. H., Yu, Y., Lan, F. N., Shan, Z. J., Sun, Y. J., Liu, P., Tang, X. B., & Rodrigo-Comino, J. (2020). Anthropogenic disturbance and precipitation affect karst sediment discharge in the Nandong underground river system in Yunnan, Southwest China. *Sustainability, 12*, 3006. https://doi.org/10.3390/su12073006.

Lizaga, I., Gaspar, L., Quijano, L., Dercon, G., & Navas, A. (2019). NDVI, (137)Cs and nutrients for tracking soil and vegetation development on glacial landforms in the Lake Paron Catchment (Cordillera Blanca, Peru). *Science of the Total Environment, 651*(Pt 1), 250–260. https://doi.org/10.1016/j.scitotenv.2018.09.075.

Lobb, D. A., & Kachanoski, R. G. (1999). Modelling tillage translocation using step, linear-plateau and exponential functions. *Soil & Tillage Research, 51*, 317–330.

López-Vicente, M., Quijano, L., Palazón, L., Gaspar, L., & Navas, A. (2015). Assessment of soil redistribution at catchment scale by coupling a soil erosion model and a sediment connectivity index (central spanish pre-pyrenees). *Cuadernos de Investigación Geográfica, 41*(1), 127–147. https://doi.org/10.18172/cig.2649.

Lu, S. H., Li, X. K., Xu, G. P., Huang, P. Z., Li, D. X., & Jiang, Z. C. (2016). Assessment of soil erosion on the typical hilly upland of Xijiang river basin based on Cs-137 tracer method. *Journal of Soil and Water Conservation, 30*(2), 38–43.

Luo, W., Jiang, Z., Yang, Q., Li, Y., & Liang, J. (2018). The features of soil erosion and soil leakage in karst peak-cluster areas of Southwest China. *Journal of Groundwater Science and Engineering, 6*(1), 18–30. https://doi.org/10.19637/j.cnki.2305-7068.2018.01.003.

Mabit, L., Martin, P., Jankong, P., Toloza, A., Padilla-Alvarez, R., & Zupanc, V. (2010). Establishment of control site baseline data for erosion studies using radionuclides: a case study in East Slovenia. *Journal of Environmental Radioactivity, 101*(10), 854–863. https://doi.org/10.1016/j.jenvrad.2010.05.008.

Marques, M., Ruiz-Colmenero, M., Bienes, R., García-Díaz, A., & Sastre, B. (2020). Effects of a permanent soil cover on water dynamics and wine characteristics in a steep vineyard in the Central Spain. *Air, Soil and Water Research, 13*, 1178622120948069. https://doi.org/10.1177/1178622120948069.

Mokhtari Karchegani, P., Ayoubi, S., Lu, S. G., & Honarju, N. (2011). Use of magnetic measures to assess soil redistribution following deforestation in hilly region. *Journal of Applied Geophysics, 75*(2), 227–236. https://doi.org/10.1016/j.jappgeo.2011.07.017.

Nearing, M. A., Kimoto, A., Nichols, M. H., & Ritchie, J. C. (2005). Spatial patterns of soil erosion and deposition in two small, semiarid watersheds. *Journal of Geophysical Research - Earth Surface, 110*(F4), 1–11. https://doi.org/10.1029/2005jf000290.

Panagos, P., Meusburger, K., Ballabio, C., Borrelli, P., & Alewell, C. (2014). Soil erodibility in Europe: a high-resolution dataset based on LUCAS. *Science of the Total Environment, 479–480*, 189–200. https://doi.org/10.1016/j.scitotenv.2014.02.010.

Parsons, A. J., & Foster, I. D. L. (2011). What can we learn about soil erosion from the use of 137Cs? *Earth-Science Reviews, 108*(1–2), 101–113. https://doi.org/10.1016/j.earscirev.2011.06.004.

Parsons, A. J., Bracken, L., Poeppl, R. E., Wainwright, J., & Keesstra, S. D. (2015). Introduction to special issue on connectivity in water and sediment dynamics. *Earth Surface Processes and Landforms, 40*(9), 1275–1277. https://doi.org/10.1002/esp.3714.

Porto, P., & Walling, D. E. (2012). Validating the use of 137Cs and 210Pbex measurements to estimate rates of soil loss from cultivated land in southern Italy. *Journal of Environmental Radioactivity, 106*, 47–57. https://doi.org/10.1016/j.jenvrad.2011.11.005.

Prise, M., Waele, J. D., & Gutierrez, F. (2009). Current perspectives on the environmental impacts and hazards in karst. *Environmental Geology, 58*, 235–237. https://doi.org/10.1007/s00254-008-1608-2.

Rahimi, M. R., Ayoubi, S., & Abdi, M. R. (2013). Magnetic susceptibility and Cs-137 inventory variability as influenced by land use change and slope positions in a hilly, semiarid region of west-central Iran. *Journal of Applied Geophysics, 89*, 68–75. https://doi.org/10.1016/j.jappgeo.2012.11.009.

Rayamajhi, N., & Manandhar, B. (2020). Impact of climate change and adaptation measures on transhumance herding system in Gatlang, Rasuwa. *Air, Soil and Water Research, 13*, 1178622120951173. https://doi.org/10.1177/1178622120951173.

Ribolzi, O., Patin, J., Bresson, L. M., Latsachack, K. O., Mouche, E., Sengtaheuanghoung, O., Silvera, N., Thiébaux, J. P., & Valentin, C. (2011). Impact of slope gradient on soil surface features and infiltration on steep slopes in northern Laos. *Geomorphology, 127*, 53–63. https://doi.org/10.1016/j.geomorph.2010.12.004.

Rodrigo-Comino, J., Ruiz Sinoga, J. D., Senciales González, J. M., Guerra-Merchán, A., Seeger, M., & Ries, J. B. (2016). High variability of soil erosion and hydrological processes in Mediterranean hillslope vineyards (Montes de Málaga, Spain). *Catena, 145*, 274–284. https://doi.org/10.1016/j.catena.2016.06.012.

Rodrigo-Comino, J., Keesstra, S., & Cerdà, A. (2018). Soil erosion as an environmental concern in vineyards: the case study of Celler del Roure, eastern Spain, by means of rainfall simulation experiments. *Beverages, 4*(2), 31. https://doi.org/10.3390/beverages4020031.

Rodrigo-Comino, J., Giménez-Morera, A., Panagos, P., Pourghasemi, H. R., Pulido, M., & Cerdà, A. (2020). The potential of straw mulch as a nature-based solution for soil erosion in olive plantation treated with glyphosate: a biophysical and socioeconomic assessment. *Land Degradation & Development, 31*(15), 1877–1889. https://doi.org/10.1002/ldr.3305.

Salesa, D., Terol, E., & Cerda, A. (2019). Soil erosion on the "El Portalet" mountain trails in the Eastern Iberian Peninsula. *Science of the Total Environment, 661*, 504–513. https://doi.org/10.1016/j.scitotenv.2019.01.192.

Schuller, P., Walling, D. E., Sepulveda, A., Trumper, R. E., Rouanet, J. L., Pino, I., & Castillo, A. (2004). Use of ^{137}Cs measurements to estimate changes in soil erosion rates associated with changes in soil management practices on cultivated land. *Applied Radiation and Isotopes, 60*(5), 759–766. https://doi.org/10.1016/j.apradiso.2003.11.087.

Smetanová, A., Paton, E. N., Maynard, C., Tindale, S., Fernández-Getino, A. P., Pérez, M. J. M., Bracken, L., Bissonnais, Y. L., & Keesstra, S. D. (2018). Stakeholders' perception of the relevance of water and sediment connectivity in water and land management. *Land Degradation & Development, 29*(6), 1833–1844. https://doi.org/10.1002/ldr.2934.

Sparks, D.L., Page, A., Helmke, P., Loeppert, R., Soltanpour, P., Tabatabai, M., Johnston, C., Sumner, M.. (1996). Methods of soil analysis. Part 3-Chiemical methods. Soil Science Society of America Inc.

Wang, S., Liu, J., Yu, G., Pan, Y., Li, K., & Li, J. (2004a). Effects of land use change on the storage of soil Forest Experimental Station in China. *Climate Change, 67*(2002), 247–255.

Wang, S. J., Li, R. L., Sun, C. X., Zhang, D. F., Li, F. Q., Zhou, D. Q., Xiong, K. N., & Zhou, Z. F. (2004b). How types of carbonate rock assemblages constrain the distribution of karst rocky desertified land in Guizhou Province, PR China: phenomena and mechanisms. *Land Degradation & Development, 15*(2), 123–131. https://doi.org/10.1002/ldr.591.

Wang, Y., Zhang, H., Zhang, G., Wang, B., Peng, S., He, Y., et al. (2017). Zoning of environmental geology and functions in karst fault-depression basins. *Carsologica Sinica, 36*(3), 283–295.

Ward, A. D., Rausch, D. L., Haan, C. T., & Heinemann, H. G. (1981). A verification study on a reservoir sediment deposition model. *American Society of Agricultural Engineers, 24*, 340–360.

Xiong, K., Yin, C., & Ji, H. (2018). Soil erosion and chemical weathering in a region with typical karst topography. *Environmental Earth Sciences, 77*(13), 500. https://doi.org/10.1007/s12665-018-7675-0.

Zebari, M., Grützner, C., Navabpour, P., & Ustaszewski, K. (2019). Relative timing of uplift along the Zagros Mountain front flexure (Kurdistan region of Iraq): constrained by geomorphic indices and landscape evolution modeling. *Solid Earth, 10*(3), 663–682. https://doi.org/10.5194/se-10-663-2019.

Zhang, X., Higgitt, D. L., & Walling, D. E. (1990). A preliminary assessment of the potential for using caesium-137 to estimate rates of soil erosion in the Loess Plateau of China. *Hydrological Sciences Journal, 35*(3), 243–252. https://doi.org/10.1080/02626669009492427.

Zhang, X., Long, Y., He, X., Fu, J., & Zhang, Y. (2008a). A simplified 137Cs transport model for estimating erosion rates in undisturbed soil. *Journal of Environmental Radioactivity, 99*(8), 1242–1246. https://doi.org/10.1016/j.jenvrad.2008.03.001.

Zhang, M. L., Yang, H., Gao, M., Yang, J. D., & Liu, X. H. (2008b). Study on soil erosion in dianchi catchment using ^{137}Cs tracer. *Acta Pedologica Sinica, 45*(6), 1017–1025.

Zhang, X. N., Wang, K. L., Zhang, W., Chen, H. S., He, X. Y., & Zhang, X. B. (2009a). Distrubution of ^{137}Cs and relative influencing factors on typical karst sloping land. *Environmental Sciences, 30*(11), 3152–3158. https://doi.org/10.13227/j.hjkx.2009.11.002.

Zhang, M. L., Yang, H., Wang, X. L., Wang, Y. H., Xu, C. A., Yang, J. D., et al. (2009b). Soil 137Cs background values in monsoon region of China. *Journal of Nuclear Agricultural Sciences, 23*(4), 669–675.

Zhang, X., Bai, X., & Liu, X. (2010). Application of a 137Cs fingerprinting technique for interpreting responses of sediment deposition of a karst depression to deforestation in the Guizhou Plateau, China. *Science China Earth Sciences, 54*(3), 431–437. https://doi.org/10.1007/s11430-010-4105-x.

Gyasi-Agyei, Y. (2006). Erosion risk assessment of controlled burning of grasses established on steep slopes. *Journal of Hydrology 317* (3-4), 276–290

Publisher's note Springer Nature remains neutral with regard to jurisdictional claims in published maps and institutional affiliations.